ELSEVIER

Dyes and Pigments 50 (2001) 133–150

DYES and PIGMENTS

www.elsevier.com/locate/dyepig

Metabolites of monomethoxy-4-aminoazobenzene dyes: a computational study

Krishna L. Bhat, Ashish Garg, Mendel Trachtman, Charles W. Bock*

Department of Chemistry, School of Science and Health and School of Textiles and Materials Technology, Philadelphia University, School House Lane and Henry Avenue, Philadelphia, PA 19144, USA

Received 6 April 2001; accepted 10 May 2001

Abstract

We report the results of a computational study of the possible metabolites of 4-aminoazobenzene (AAB) and its monomethoxy derivatives using density functional theory (DFT) and the semiempirical AM1 method. These calculations identify several factors that may influence the radically different carcinogenic activities of 2-methoxy-and 3-methoxy-AAB.

Keywords: Aminoazobenzene dyes; Metabolites; Density functional theory (DFT)

1. Introduction

Chemical carcinogens comprise a large, structurally diverse group of naturally occurring and synthetic organic and inorganic compounds. The majority of known carcinogens are low molar mass (< 500 amu) organic compounds and they include a variety of polycyclic aromatic hydrocarbons, aromatic amines, dialkyl nitrosamines, alkyl nitrosamides, polychlorinated aliphatic and alicyclic hydrocarbons, aflatoxins, pyrrolizidine alkaloids and a wide array of alkylating agents. The lack of a common structural feature among the chemical carcinogens and the ability of some, e.g. aromatic amines, to produce tumors at distant sites such as the liver and urinary bladder (regardless of the route of administration) has led to the conclusion that many of these chemicals are not carcinogens per se, but require activation via a series of metabolic transformations [1].

In this work we are concerned with the properties of various metabolites of 4-aminoazobenzene (AAB, C. I. Solvent Yellow) and *n*-methoxy-4-aminoazobenzene (*n*-OMe–AAB). These dyes exhibit a broad spectrum of carcinogenic/mutagenic activity, e.g. 3-OMe–AAB is a potent hepatocarcinogen in the rat [2], whereas 2-OMe–AAB is a noncarcinogen under similar conditions; neither of these dyes, however, is mutagenic per se in the *Salmonella typhimuriuin* strains TA98 or TA 100. The origin of such divergent behavior is not known.

It is generally believed that AAB dyes, like the majority of aromatic amines, are activated through biotransformation at their extracyclic amino group. Evidence suggests that the first step

* Corresponding author. Tel.: +1-215-951-2876; fax: +1-215-951-6812.

E-mail address: chuck@larry.philau.edu (C.W. Bock).

0143-7208/01/$ - see front matter
PII: S0143-7208(01)00032-8

in this metabolic activation is *N*-hydroxylation, a result of enzymatic *N*-oxidation reactions [3]. These reactions are catalyzed preferentially by cytochromes P450IA2 and P450IIIA or by the flavin-containing mono-oxygenases [4]. The precise mechanism by which this transformation occurs at physiological temperatures appears to be rather complex and it is not well understood [5,6]. Our recent DFT calculations [7,8] on AAB, the positional isomers of OMe–AAB and their *N*-hydroxy derivatives suggest that the overall thermodynamics of *N*-hydroxylation is not significantly affected by substitution of a methoxy group at any position on either phenyl ring in AAB. The results of these calculations are in accord with the semiempirical AM1 calculations of Ford and Herman [9] who found that the nature of the aryl moiety in a wide variety of arylamines had relatively little effect on the reaction energetics of *N*-hydroxylation. There are indications, however, that the rate of *N*-hydroxylation of AAB-based dyes may be sensitive to the position of substituents on the rings, e.g. Kimura et al. [10] observed that the rate of *N*-hydroxylation in 3′-methyl-*N*-methyl-4-aminoazobenzene (3′-Me–MAB) is about three times greater than that for 4′-Me–MAB. Furthermore, there appears to be some correlation between the rate of formation of N–OH–MAB dyes and the carcinogenic activity of their corresponding DAB derivatives [10], although rate data are available for only about 10 compounds.

Using the Gene-Tox *Salmonella* mutagenicity data base [11] and their computer-automated structure evaluation (CASE) methodology, Rosenkranz and Klopman [12,13] found that the presence of the structural fragment CH=CH–CH=CH–N=N–CH=CH– in a molecule was an activating factor (biophore) for mutagenicity. These authors suggested that this fragment may be a recognition site for the enzymes involved in *N*-hydroxylation. Interestingly, this fragment appears twice in 3′-Me–MAB but not at all in 4′-Me–MAB and the 3′-isomer is about ten times more carcinogenic than the 4′-isomer [10]. This same structural fragment appears four times in the potent carcinogen 3-OMe–AAB but only twice in the non-carcinogen 2-OMe–AAB. Although the presence of this fragment may be an activating structural feature, it is not the only factor influencing the carcinogenic behavior of azobenzene compounds since this fragment is present four times in AAB itself which is only a weak carcinogen.

For a few aromatic amines their *N*-hydroxy metabolites are sufficiently electrophilic per se at acid to neutral pH that they can bind directly to electron rich biotargets in vitro [14,15]. However, for most aromatic amines and AAB dyes further metabolic activation appears to be required [16]. This is in accord with results from our recent calculations [7,8]. We found, for example, in going from 2(3)-OMe–AAB to N–OH–2(3)–OMe–AAB that the energy of the lowest unoccupied molecular orbital (LUMO) decreases by only 4.1 (4.4)%, suggesting that *N*-hydroxylation has relatively little effect on the electrophilic nature of these dyes.

If the *N*-hydroxy derivative is formed, it would be susceptible to a rich variety of further metabolic processes [17]. There is evidence [18] that N–OH–AAB compounds undergo metabolic activation to form highly reactive N–O esters, see Scheme 1. These esterifications are catalyzed by enzymes such as sulfotransferases and acetyltransferase [4]. Little is known, however, about factors that influence the rate of formation of these esters from their N–OH–AAB precursors. In an aqueous environment under physiological pH these esters presumably undergo rate-limiting N–O bond cleavage during solvolysis [19] to produce highly electrophilic nitrenium ions that can react directly with DNA [19,20], especially at guanine residues. Covalent modification of DNA is the first step in chemical carcinogenesis [21] and if such modifications are not repaired, the fidelity of DNA replication may be compromised, leading to mutations and possibly cancer [22]. However, the formation of only a few covalent adducts have been studied [23] and there is conflicting evidence as to the detailed nature of the mechanism by which the adduct is formed [24]. In order for nitrenium ions to efficiently interact with the DNA or other cellular nucleophiles, it is important that they are trapped by solvent molecules at a sufficiently slow rate. It has been shown that esters derived from some strongly carcinogenic and

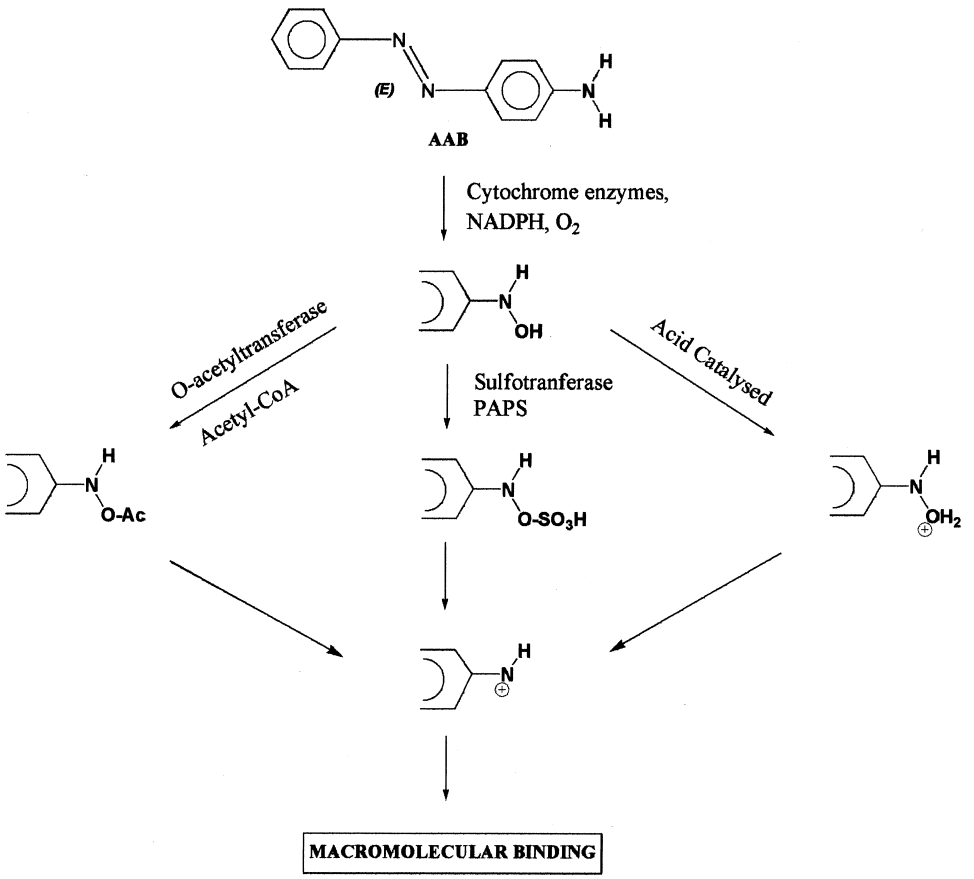

Scheme 1.

mutagenic amines, such as 2-aminofluorene (2-AF) and 4-aminobiphenyl, produce long-lived nitrenium ions that selectively react with deoxyguanasine in the presence of an aqueous solvent [25–30]. No corresponding experimental data is currently available for nitrenium ions derived from AAB dyes. Additional metabolic pathways for AAB compounds include detoxification mechanisms, such as ring hydroxylation [31].

The purpose of the present paper is to describe the results of an extensive computational study using density functional theory (DFT) and the semiempirical AM1 method on various metabolites of AAB and *n*-OMe–AAB. In particular, we report structural, electronic and energetic data on several esters and nitrenium ions derived from AAB and OMe–AAB. These results augment those we have published previously for AAB, *n*-OMe–AAB and their *N*-hydroxy derivatives [7,8]. The ultimate goal of this work is to identify *computational* procedures that would enable the rapid screening of dyes for possible carcinogenic activity.

2. Computational methods

Density functional calculations were performed at the BP/DN** computational level with SPARTAN v5.0 on Silicon Graphics computers [32]. This level uses the non-local Becke–Perdew (BP) 86 functional and employs the numerically defined DN** basis set which includes polarization functions on all the atoms [33,34]. Complete optimiza-

tions for a variety of potential metabolites of AAB and their methoxy derivatives were carried out. No symmetry constraints were employed in the calculations in order to minimize the likelihood of optimizing to a transition state. In a few cases, frequency analyses were performed to ensure that the optimized structures were local minima on the potential energy surfaces (PESs). The graphics utilities of SPARTAN were used extensively to examine the electron densities, electrostatic potentials and Kohn–Sham orbitals for a variety of conformers of each of the dyes and their metabolites that we considered [32]. Atomic charges derived from the electrostatic potential were also calculated for all the structures included in this study. For comparison, we also performed a few optimizations at the B3LYP/6-31+G* computational level [35] using the GAUSSIAN 98 series of programs [36].

We also carried out a series of calculations on AAB and its methoxy derivatives using the programming package CODESSA [37] in conjunction with the semiempirical AM1 method implemented in AMPAC 5.0 [38]. This package allows for the calculation of a wide variety of molecular descriptors based on 3D geometrical and quantum chemical information, and it has been used successfully for developing quantitative structure/activity and structure/property relationships (QSAR, QSPR) in a wide variety of applications [39–41].

3. Results and discussion

In Table 1 [42] we report total molecular energies, Kohn–Sham frontier molecular orbital energies, bond lengths involving the extracyclic amino nitrogen and selected electronic properties of AAB and a variety of its proposed metabolites: N–OH–AAB, N–OAc–AAB, N–OSO_3H–AAB (N–OSO_3^-–AAB), and the nitrenium ion $^+$NH–AAB ([$^+$NH–AAB]·H_2O). Corresponding results for the *n*-methoxy ($n=2$, 3, 5 and 6) derivatives of these metabolites are also given in Table 1. Since the two hydrogen atoms on the amine group in AAB are not equivalent, *N*-substitution requires consideration of two distinct forms. We will refer to these two forms as *syn* and *anti*; their optimized structures are shown for N–OAc–AAB in Fig. 1 along with the numbering system we are using. Energy differences between the lowest-energy *syn* and the lowest-energy *anti* forms can differ by several kcal/mol, see Table 1B and C. Total molecular energies of the small molecules used to compute various reaction energies in later tables are given in Table 1D.

Table 2A [43–46] lists the available carcinogenic/mutagenic data for AAB and a few of its metabolites. Since the data are quite sparse we have included the corresponding data for *n*-OMe–AAB and MAB in Table 2B and C respectively. It appears from Table 2 that *N*-hydroxylation increases the mutagenic potency of these types of compounds [44,45], although in some cases the increase is marginal. Data on the effects of esterification are available only for MAB and in this case there is a significant increase in the mutagenicity of N–OAc–MAB compared to that of either MAB or N–OH–MAB, see Table 2C. Esterification of *N*-hydroxy-2-acetamido-fluorene (N–OH–2-AAF), derived from the potent carcinogen 2-AF, has also been studied [47] and N–OAc–2-AAF has been found to be a more powerful carcinogen locally than N–OH–2-AAF.

3.1. $AAB \rightarrow N\text{–}OH\text{–}AAB \rightarrow N\text{–}OAc(OSO_3H)\text{–}AAB \rightarrow {}^+NH\text{–}AAB$

We initially optimized a variety of possible metabolites of AAB itself, in order to establish a baseline of typical behavior; AAB is a weak carcinogen [43,44]. It is important to note that neither *N*-hydroxylation nor *N*-esterification dramatically changes the calculated structure of the azobenzene backbone found in AAB, e.g. corresponding bond lengths in the phenyl rings of AAB, N–OH–AAB and N–OAc(–OSO_3H)–AAB are very similar and these rings remain nearly in the same plane; selected torsional angles for these metabolites are listed in Table 3A. Furthermore, the structure at the amino nitrogen atom is consistently pyramidal for all these molecules.

In Fig. 2 we compare several properties of the *syn* forms of AAB, N–OH–AAB, N–OAc–AAB and $^+$NH–AAB; similar results are obtained for

Table 1
Total molecular energies (a.u.), Kohn–Sham frontier orbital energies (a.u.), bond lengths (Å), electrostatic charges, dipole moments (D) and log *P* (octanol–water partition coefficient) of A. AAB and *n*-OMe–AAB, B. *Syn* N–OH–AAB, N–OAc–AAB, N–OSO_3H–AAB, N–OSO_3^-–AAB, $^+$NH–AAB, [$^+$NH–AAB]·H_2O and their corresponding *n*-methoxy derivatives, C. *anti* N–OH–AAB, N–OAc–AAB, $NOSO_3H$–AAB, N–OSO_3^-–AAB, $^+$NH–AAB, [$^+$NH–AAB]·H_2O and their corresponding *n*-methoxy derivatives ($n = 2$, 3, 5 and 6), D. small molecules used to compute reaction energies[a,b,c]

Compound	Energies (a.u.)				Bond lengths (Å)		Charges			Dipole moment (D)	Log *P*
	Total	HOMO{-1}	HOMO	LUMO	C_4–N	N–O	C_4	(C_4)N	(N)O		
A.											
AAB	−628.365269	−0.192206[a]	−0.187648[b]	−0.111910	1.388	–	+0.29	−0.72	–	3.61	3.67
2-OMe–AAB	−742.931707	−0.186667[a]	−0.172130[b]	−0.101149	1.390	–	+0.33	−0.73	–	4.81	3.54
3-OMe–AAB	−742.942471	−0.186267[b]	−0.184347[a]	−0.109143	1.380	–	+0.13	−0.67	–	3.51	3.54
5-OMe–AAB	−742.941042	−0.185290[b]	−0.183553[a]	−0.109506	1.384	–	+0.13	−0.67	–	3.54	3.54
6-OMe–AAB	−742.936054	−0.185048[a]	−0.179274[b]	−0.106652	1.390	–	+0.34	−0.72	–	5.08	3.54
B. Syn											
N-OH–AAB	−703.568693	−0.198135	−0.191581	−0.117278	1.404	1.439	+0.48	−0.54	−0.39	2.55	3.64
2-OMe–N–OH–AAB	−818.135537	−0.190880	−0.175956	−0.105674	1.405	1.437	+0.47	−0.51	−0.39	4.06	3.52
3-OMe–N–OH–AAB	−818.140454	−0.195636	−0.195078	−0.121241	1.403	1.455	+0.28	−0.56	−0.37	1.40	3.52
5-OMe–N–OH–AAB	−818.143086	−0.189639	−0.188680	−0.114688	1.397	1.439	+0.30	−0.49	−0.38	2.79	3.52
6-OMe–N–OH–AAB	−818.141158	−0.191280	−0.183861	−0.112430	1.407	1.438	+0.52	−0.53	−0.39	3.95	3.52
N–OAc–AAB	−856.292894	−0.204314	−0.195007	−0.120974	1.414	1.445	+0.32	−0.42	−0.19	2.10	3.72
2-OMe–N–OAc–AAB	−970.859136	−0.196645	−0.178600	−0.110300	1.417	1.450	+0.31	−0.41	−0.19	3.89	3.59
3-OMe–N–OAc–AAB	−970.865441	−0.201745	−0.196886	−0.123252	1.410	1.471	+0.13	−0.43	−0.23	2.76	3.59
5-OMe–N–OAc–AAB	−970.867551	−0.195020	−0.192163	−0.118250	1.408	1.443	+0.13	−0.38	−0.19	0.84	3.59
6-OMe–N–OAc–AAB	−970.864538	−0.196353	−0.186659	−0.115798	1.414	1.448	+0.36	−0.42	−0.19	2.31	3.59
N–OSO_3H–AAB	−1327.599879	−0.217793	−0.204853	−0.132345	1.411	1.459	+0.31	−0.48	−0.14	3.37	3.48
2-OMe–N–OSO_3H–AAB	−1442.165189	−0.208197	−0.187410	−0.121210	1.412	1.454	+0.34	−0.41	−0.23	2.71	3.36
3-OMe–N–OSO_3H–AAB	−1442.171846	−0.211521	−0.205516	−0.132988	1.408	1.465	+0.10	−0.39	−0.25	4.81	3.36
5-OMe–N–OSO_3H–AAB	−1442.176097	−0.207178	−0.202296	−0.129319	1.407	1.456	+0.10	−0.35	−0.23	4.08	3.36
6-OMe–N–OSO_3H–AAB	−1442.169895	−0.208135	0.196956	−0.128055	1.413	1.461	+0.36	−0.42	−0.23	2.75	3.36
N–OSO_3^-–AAB	−1327.123895	−0.097769	−0.082062	−0.023094	1.362	1.388	+0.46	−0.42	−0.28	18.19	–
2-OMe–N–OSO_3^-–AAB	−1441.693278	−0.086882	−0.080997	−0.014937	1.368	1.025	+0.40	−0.41	−0.29	16.51	–
3-OMe–N–OSO_3^-–AAB	−1441.686910	−0.092628	−0.075955	−0.021692	1.365	1.382	+0.33	−0.36	−0.29	17.33	–
5-OMe–N–OSO_3^-–AAB	1441.696723	−0.095736	−0.075829	−0.020404	1.354	1.381	+0.25	−0.32	−0.29	18.05	–
6-OMe–N–OSO_3^-–AAB	−1441.692972	−0.092506	−0.080343	−0.019328	1.362	1.390	+0.48	−0.41	−0.29	17.81	–
[$^+$NH–AAB]·H_2O	−703.936838	−0.367408	−0.364003	−0.316667	1.302	2.995	+0.71	−0.71	−0.80	1.55	3.56
2-OMe–[$^+$NH–AAB]·H_2O	−818.516345	−0.353515	−0.347905	−0.305783	1.304	3.061	+0.73	−0.73	−0.83	2.41	3.43
3-OMe–[$^+$NH–AAB]·H_2O	−818.524846	−0.359266	−0.352627	−0.304348	1.292	2.972	+0.57	−0.72	−0.83	0.87	3.43
5-OMe–[$^+$NH–AAB]·H_2O	−818.521664	−0.362283	−0.352437	−0.303698	1.292	3.085	+0.55	−0.66	−0.77	1.86	3.43
6-OMe–[$^+$NH–AAB]·H_2O	−818.518040	−0.357859	−0.351185	−0.308611	1.304	3.043	+0.75	−0.73	−0.83	1.72	3.43
$^+$NH–AAB	−627.453548	−0.384208	−0.377843	−0.325857	1.302	–	+0.56	−0.60	–	1.91	3.94
2-OMe–$^+$NH–AAB	−742.033931	−0.370146	−0.357127	−0.312471	1.303	–	+0.58	−0.62	–	3.02	3.82
3-OMe–$^+$NH–AAB	−742.041900	−0.379054	−0.362473	−0.312818	1.292	–	+0.41	−0.59	–	1.56	3.82
5-OMe–$^+$NH–AAB	−742.042492	−0.380976	−0.362483	−0.311252	1.292	–	+0.41	−0.56	–	2.51	3.82
6-OMe–$^+$NH–AAB	−742.035068	−0.374847	−0.361200	−0.318203	1.305	–	+0.61	−0.63	–	2.41	3.82

(Table continued on next page)

Table 1 (*continued*)

Compound	Energies (a.u.)				Bond lengths (Å)		Charges			Dipole moment (D)	Log *P*
	Total	HOMO{-1}	HOMO	LUMO	C_4–N	N–O	C_4	(C_4)N	(N)O		
C. Anti											
N–OH–AAB	−703.569992	−0.199456	−0.192288	−0.117499	1.405	1.441	+0.52	−0.57	−0.39	2.36	3.64
2-OMe–N–OH–AAB	−818.135954	−0.191485	−0.175900	−0.106489	1.406	1.435	+0.51	−0.54	−0.40	3.89	3.52
3-OMe–N–OH–AAB	−818.145385	−0.194489	−0.189757	−0.113902	1.397	1.433	+0.29	−0.47	−0.38	2.80	3.52
5-OMe–N–OH–AAB	−818.139130	−0.195457	−0.193532	−0.121805	1.404	1.459	+0.27	−0.59	−0.38	1.65	3.52
6-OMe–N–OH–AAB	−818.140274	−0.189450	−0.182742	−0.110815	1.405	1.436	+0.48	−0.52	−0.39	3.91	3.52
N–OAc–AAB	−856.292321	−0.210821	−0.197700	−0.124478	1.419	1.465	+0.31	−0.47	−0.22	1.87	3.72
2-OMe–N–OAc–AAB	−970.857128	−0.200722	−0.181297	−0.112691	1.418	1.461	+0.32	−0.46	−0.22	2.13	3.59
3-OMe–N–OAc–AAB	−970.868784	−0.201312	−0.194520	−0.120933	1.413	1.458	+0.10	−0.39	−0.22	1.37	3.59
5-OMe–N–OAc–AAB	−970.861704	−0.201032	−0.197997	−0.124127	1.413	1.482	+0.13	−0.47	−0.23	3.07	3.59
6-OMe–N–OAc–AAB	−970.862465	−0.199942	−0.187731	−0.117367	1.420	1.457	+0.33	−0.44	−0.22	3.70	3.59
N–OSO_3H–AAB	−1327.595677	−0.217166	−0.205443	−0.132628	1.408	1.444	+0.26	−0.41	−0.23	3.46	3.48
2-OMe–N–OSO_3H–AAB	−1442.160660	−0.208951	−0.189827	−0.122503	1.413	1.447	+0.28	−0.40	−0.24	3.18	3.36
3-OMe–N–OSO_3H–AAB	−1442.172024	−0.207514	−0.204022	−0.129450	1.399	1.436	+0.06	−0.33	−0.23	4.37	3.36
5-OMe–N–OSO_3H–AAB	−1442.167991	−0.210650	−0.205077	−0.132995	1.411	1.468	+0.07	−0.42	−0.24	4.71	3.36
6-OMe–N–OSO_3H–AAB	−1442.167330	−0.207118	−0.196413	−0.126920	1.410	1.440	+0.32	−0.38	−0.24	2.55	3.36
N–OSO_3^-–AAB	−1327.122020	−0.095760	−0.082976	−0.023234	1.366	1.387	+0.48	−0.45	−0.29	–	–
2-OMe–N–OSO_3^-–AAB	−1441.685818	−0.087028	−0.081054	−0.015951	1.370	1.392	+0.46	−0.44	−0.30	–	–
3-OMe–N–OSO_3^-–AAB	−1441.696453	−0.093856	−0.077383	−0.019960	1.356	1.378	+0.25	−0.32	−0.31	–	–
5-OMe–N–OSO_3^-–AAB	−1441.679704	−0.091508	−0.075590	−0.022025	1.367	1.376	+0.31	−0.38	−0.29	–	–
6-OMe–N–OSO_3^-–AAB	−1441.694473	−0.091987	−0.081477	−0.019037	1.371	1.390	+0.47	−0.41	−0.30	–	–
[$^+$NH–AAB]·H_2O	−703.934716	−0.369013	−0.360497	−0.311590	1.300	2.933	+0.70	−0.73	−0.78	–	–
2-OMe–[$^+$NH–AAB]·H_2O	−818.516853	−0.351956	−0.351465	−0.299720	1.302	3.058	+0.72	−0.74	−0.78	–	–
3-OMe–[$^+$NH–AAB]·H_2O	−818.523776	−0.359434	−0.355657	−0.304988	1.291	2.950	+0.49	−0.66	−0.79	–	–
5-OMe–[$^+$NH–AAB]·H_2O	−818.519892	−0.357061	−0.351697	−0.296432	1.290	2.981	+0.57	−0.72	−0.79	–	–
6-OMe–[$^+$NH–AAB]·H_2O	−818.515856	−0.354049	−0.349244	−0.307758	1.302	2.947	+0.72	−0.73	−0.77	–	–
$^+$NH–AAB	−627.451717	−0.384738	−0.378227	−0.327147	1.302	–	+0.57	−0.62	–	2.09	3.94
2-OMe–$^+$NH–AAB	−742.035919	−0.369977	−0.360803	−0.311225	1.303	–	+0.60	−0.65	–	3.10	3.82
3-OMe–$^+$NH–AAB	−742.042832	−0.381416	−0.350630	−0.315035	1.293	–	+0.36	−0.55	–	2.86	3.82
5-OMe–$^+$NH–AAB	−742.038930	−0.379337	−0.358915	−0.312006	1.292	–	+0.44	−0.60	–	1.70	3.82
6-OMe–$^+$NH–AAB	−742.033259	−0.374306	−0.357966	−0.317990	1.304	–	+0.61	−0.62	–	3.09	3.82
D. Energy											
H_2O	−76.471211										
H_3O^+	−76.739996										
$CH_3C(O)OH$	−229.200567										
H_2SO_4	−700.507030										
$C_6H_5C(O)OH$	−421.002404										
C_6H_5–NHOH	−362.922275										
C_6H_5–NHOAc	−515.648669										
C_6H_5–$NHSO_3H$	−986.954399										
$C_6H_5^+$–NH	−286.766 166										

[a] Orbital involves amino nitrogen lone pair of electrons.

[b] Orbital involves azo bond lone pair of electrons.

[c] Calculated using the Ghose–Crippen approach [42].

the corresponding *anti* forms. As shown in Fig. 2A, the calculated length of the C_4–N bond does not change significantly in progressing from AAB→N–OH–AAB→N–OAc–AAB; in going from N–OH–AAB to N–OAc(–OSO_3H, or –OC_6H_5)–AAB, the N–O bond length does increase, but not dramatically. The sulfate is more effective at lengthening the N–O bond than the acetate, see Table 1. On the other hand, formation of the nitrenium ion is accompanied by significant structural changes. In particular, the azobenzene backbone of the nitrenium ion is substantially twisted, see Table 3A. The length of the C_4–N bond in this ion, 1.302 Å, shows a significant double bond character, and the N–H bond is essentially in the plane of the phenyl ring to which it is attached. Furthermore, differences in the lengths of the formal single and double bonds found in the phenyl rings of $^{+}$NH–AAB are much more pronounced than that found in AAB, N–OH–AAB or N–OAc–AAB.

In Fig. 2B we show the changes in the energies of the frontier orbitals along this metabolic pathway. The Kohn–Sham highest occupied molecular

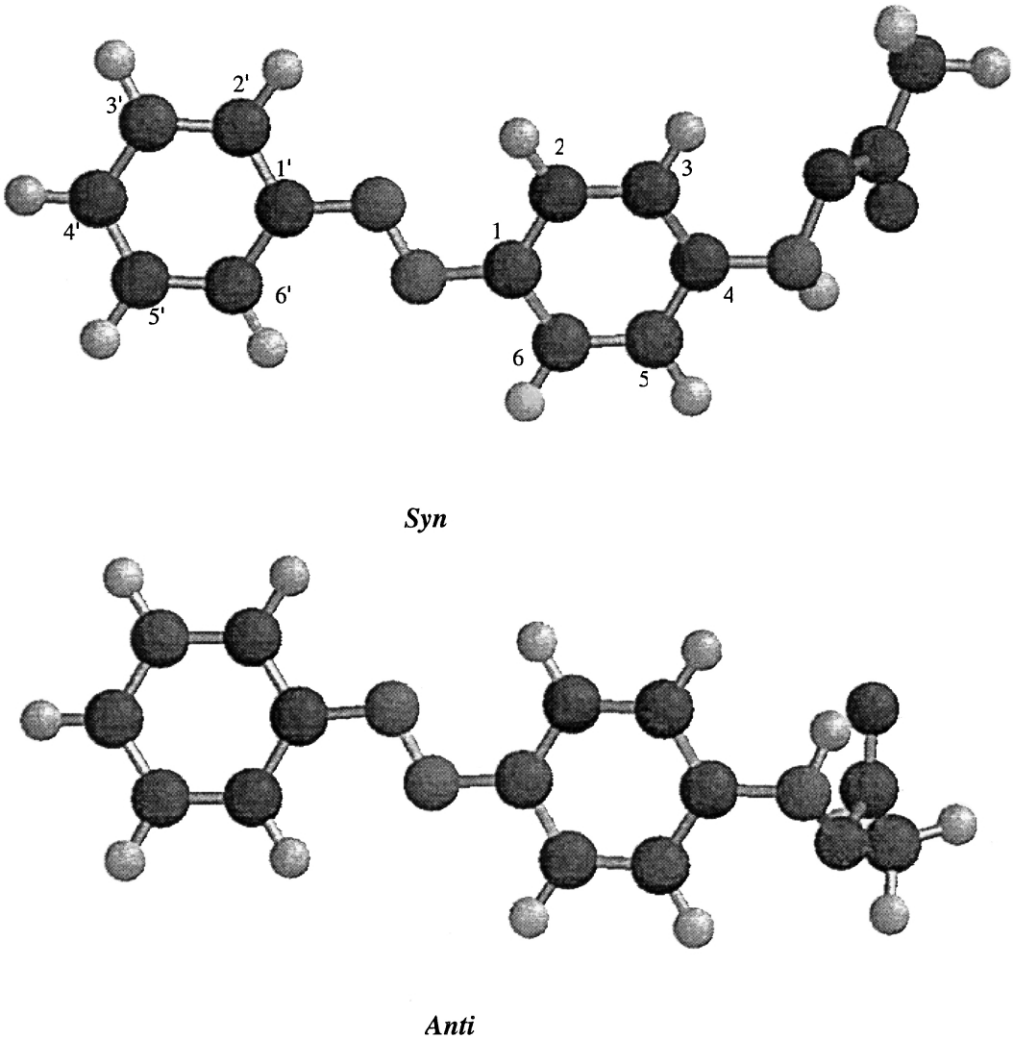

Fig. 1. The *syn* and *anti* optimized structures of N–OAc–AAB calculated at the BP/DN**//BP/DN** computational level.

orbital (HOMO) for AAB, N–OH–AAB and N–OAc–AAB (as well as, for N–OSO_3H–AAB and N–OBz–AAB) is predominantly localized in the region of the azo lone pairs of electrons. The HOMO{-1} is essentially pi-bonding for the azobenzene backbone with a contribution in the vicinity of the amino lone pair of electrons. The LUMO in these structures is pi-antibonding for the backbone. These orbitals are shown for N–OAc–AAB in Fig. 3A. It is evident from Fig. 2B that the frontier orbital energies decrease slightly along the pathway: AAB→N–OH–AAB→N–OAc–AAB. (When OSO_3H is used in place of OAc the HOMO{-1}, HOMO and LUMO are lower in energy by 0.37, 0.27 and 0.31 eV respectively). The separation in energy between the two

Table 2
Carcinogenic/mutagenic behavior of various metabolites of A. AAB, B. *n*-OMe-AAB and C. MAB

Compound	Carcinogenicity		Mutagenicity revertants (nmol/dye)				References
	Rat	Mouse	TA 98		TA 100		
			S-9(−)	S-9(+)	S-9(−)	S-9(+)	
A.							
AAB	Very weak	ND	0	0.07	0	0.80	43
			0.03	0.20	0.29	0.61	
			0.08	0.36	0.52	0.89	44
			0.25	0.79	1.31	1.58	
				0.23		0.70	
				0.16		0.42	45
				0.11		0.41	
N–OH–AAB	ND	ND	0.07	1.03	0	0.72	43
N–OAc–AAB	ND	ND	ND	ND	ND	ND	
N–OSO_3H–AAB	ND	ND	ND	ND	ND	ND	
B.							
2-OMe–AAB	None	ND	0	0.01	0	0.08	43
N–OH-2-OMe–AAB	ND	None	0.11	0.04	0	0.09	43
N–OAc-2-OMe–AAB			0		0		
3-OMe–AAB	Strong	None (male)	0	32.20	0	31.00	43
		Weak (female)	0.31	72.96	1.41	62.68	44
N–OH-3-OMe–AAB	ND	Moderate	68.30	192.00	29.20	47.50	
			170.00		24.24		43
			88.87		18.18		
C.							
MAB	Strong	ND	0.02	0.28	0.20	0.60	
			0.08	0.37	0.42	0.77	44
			0.23	0.90	1.20	1.84	
			1.00				
			0.60				46
			0.38				
N–OH–MAB	Moderate	Moderate	3.00				
			1.30				46
			0.72				
N–OAc–MAB			25.00		50.00		46
			24.00		33.93		
N–OBz–MAB	Strong	ND	72.00	ND	76.00	ND	46
			28.57		56.00		
			10.00		12.80		

highest occupied orbitals along this path increases somewhat because the energy of the HOMO{-1} is lowered to a greater extent than that of the HOMO. As expected, formation of $^{+}$NH–AAB leads to substantial changes in the energies of the frontier orbitals. In particular, the energy of the LUMO is reduced by 5.6 eV, which is consistent with a dramatic increase in electrophilicity. The Kohn–Sham orbitals for this severely-twisted nitrenium ion are shown in Fig. 3B, where it is evident that the LUMO has a significant contribution at the amino nitrogen atom.

As can be seen in Fig. 2C, the value of the dipole moment in going from AAB→N–OH–AAB→N–OAc–AAB→ $^{+}$NH–AAB decreases monotonically, even though the changes in the calculated atomic charges are not all monotonic, see Fig. 2D. Comparison of the distribution of atomic charges in AAB and $^{+}$NH–AAB, calculated from the electrostatic potential, shows a substantial shift of electron density from both rings and the azo linkage toward the $-^{+}$NH moiety; the charge on the amino nitrogen atom in $^{+}$NH–AAB, −0.60, is more negative than that in N–OAc–AAB, −0.42, or in N–OSO_3H–AAB, −0.48. The charge density and bond lengths in $^{+}$NH–AAB emphasize the importance of the resonance structure

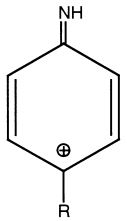

for these nitrenium ions [26].

Enzymatic formation of an N-ester from N–OH–AAB in an aqueous environment can lead to reformation of N–OH–AAB with the concomitant formation of an acid. In Table 4 A we list enthalpy changes, ΔH, for the reaction

$$\mathrm{N-OR-AAB + H_2O} \rightarrow \mathrm{N-OH-AAB + ROH}, \quad (1)$$

where R = $COCH_3$, SO_3H or COC_6H_5. These reactions are all slightly exothermic. The production of

Table 3
Magnitude of selected torsional angles (°) for the syn forms of A. AAB, N–OH–AAB, N–OAc–AAB, N–OSO_3H–AAB and $^{+}$NH–AAB and B. 2(3)-OMe–AAB, N–OH–2(3)-OMe–AAB, N–OAc-2(3)-OMe–AAB, N–OSO_3H–2(3)-OMe–AAB and $^{+}$NH-2(3)-OMe–AAB

	$\tau(C_{6'}C_{1'}NN)$	$\tau(C_{1'}NNC_1)$	$\tau(NNC_1C_2)$	$\tau(C_3C_4NH)$
A.				
AAB	0.46	179.65	0.64	161.00
N–OH–AAB	0.56	179.35	0.44	152.14
N–OAc–AAB	1.86	179.62	10.37	139.29
N–OSO_3H–AAB	11.61	178.45	1.48	169.24
N–OSO_3^-–AAB	3.60	179.57	1.33	161.25
$^{+}$NH–AAB	3.55	153.58	43.73	179.40
B.				
2-OMe–AAB	8.61	179.11	8.53	163.29
3-OMe–AAB	0.26	179.63	0.17	159.80
N–OH–2-OMe–AAB	10.46	178.90	4.64	145.93
N–OH–3-OMe–AAB	1.37	179.73	1.78	178.38
N–OAc–2-OMe–AAB	1.52	179.70	12.90	135.81
N–OAc–3-OMe–AAB	15.40	177.91	5.48	166.98
N–OSO_3H–2-OMe–AAB	10.88	178.04	1.01	166.08
N–OSO_3H–3-OMe–AAB	7.70	176.93	4.87	176.74
$^{+}$NH-2-OMe–AAB	3.05	152.65	49.08	179.68
$^{+}$NH-3-OMe–AAB	7.86	157.09	44.82	178.87

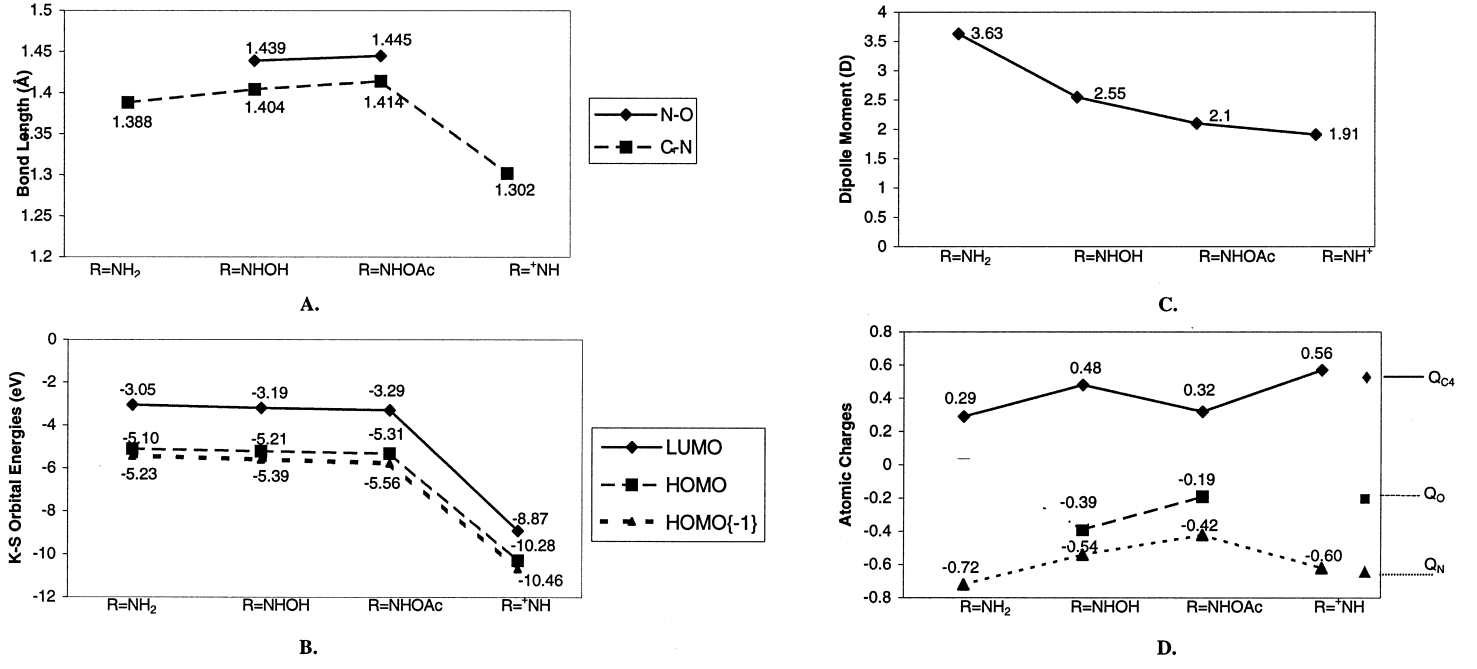

Fig. 2. Comparison of the A. C_4–N and N–O bond lengths (Å), B. frontier orbital energies (eV), C. dipole moments and D. electrostatic charges for the *syn* forms of AAB, N–OH–AAB, N–OAc–AAB and $^{+}$NH–AAB calculated at the BP/DN**//BP/DN** computational level.

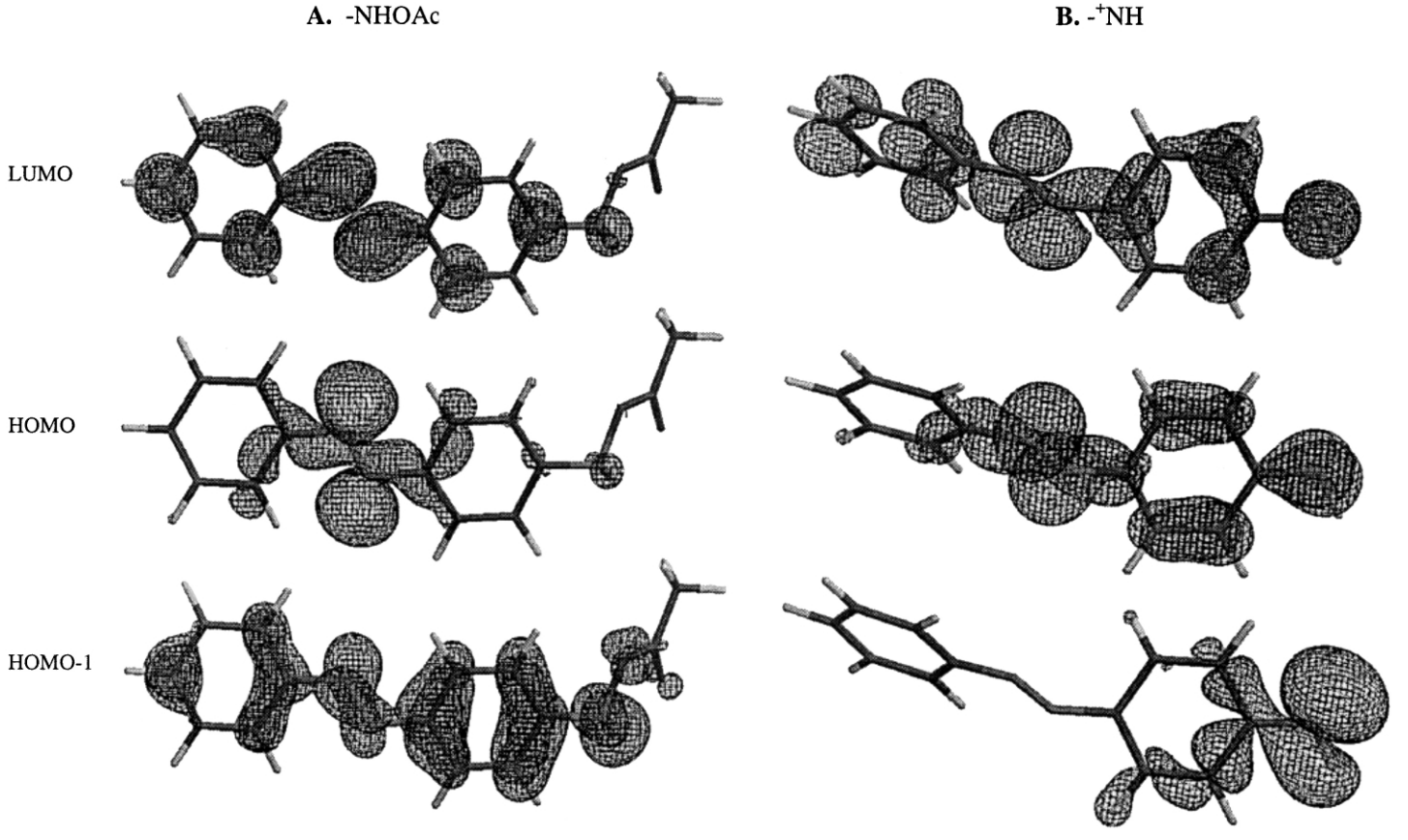

Fig. 3. The Kohn–Sham LUMO, HOMO and HOMO{-1} of A. N–OAc–AAB and B. $^{+}$NH–AAB calculated at the BP/DN**//BP/DN** computational level.

the acid ROH will lower the pH in the local environment and catalyze the formation of nitrenium ions from N–OH–AAB directly. Our calculated reaction enthalpy for the acid catalyzed formation of $^{+}$NH–AAB from N–OH–AAB is quite exothermic, −54.8 kcal/mol (H_3O^+ was used to simulate the acid in this calculation).

Since the calculated charge on the oxygen atom in N–OH–AAB is more negative than the charge on the amino nitrogen atom, see Table 1, we thought that it might be possible to form a stable structure by protonating the oxygen atom. However, several optimizations initiated from this type of structure all yielded what would best be described as a nitrenium ion–water adduct, [$^{+}$NH–AAB]·H_2O. This adduct is some 3.5 kcal/mol lower in energy than a separated nitrenium ion and a water molecule.

In Table 5A we compare the stability of nitrenium ions formed from AAB with those formed from aniline by calculating enthalpy changes for the reaction

$$\mathrm{N-OR-AAB} + {}^{+}\mathrm{NH-C_6H_5} \rightarrow {}^{+}\mathrm{NH-AAB} + \mathrm{N-OR-C_6H_5} \quad (2)$$

where R = H, Ac and SO_3H. This reaction is substantially exothermic for each of these substituents, $\Delta H \sim -25$ kcal/mol, which confirms the notion that the azobenzene backbone is very effective at stabilizing a nitrenium ion. The energetics of reaction (2) for a variety of other aryl nitrenium ions, calculated using the semiempirical AM1 method, have shown that the nature of the aryl group can have a significant effect on the stability of this ion [9]. The lifetimes of aryl nitrenium ions, especially those with highly conjugated structures, are under intense investigation because of their apparent role in DNA damage [48]. Novel experiments have shown that biphenyl and fluorenyl nitrenium ions are long-lived in water and have high deoxyguanosine:water selectivities, compared to their carbenium ion analogs, no corresponding data are currently available concerning

Table 4
Enthalpy change, ΔH (kcal/mol), for the reaction

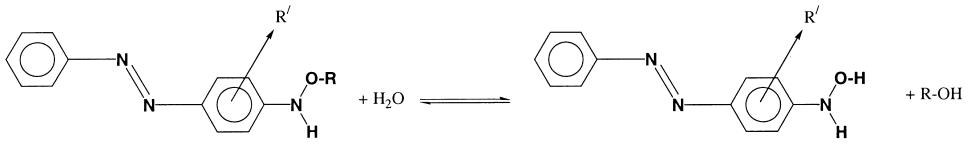

for A. R = Ac, SO_3H and Bz, R′ = H and B. R = Ac and SO_3H, R′ = 2(3)-OMe calculated at the BP/DN**//BP/DN** computational level

R	R′	ΔH (kcal/mol)	
		syn	*anti*
A.			
Ac	H	−3.2	−4.4
SO_3H	H	−2.9	−6.4
Bz	H	−5.1	–
B.			
Ac	2-OMe	−3.6	−5.1
SO_3H	2-OMe	−3.9	−7.0
Ac	3-OMe	−2.7	−3.7
SO_3H	3-OMe	−2.8	−5.8
Ac	5-OMe	−3.1	−4.3
SO_3H	5-OMe	−1.8	−4.4
Ac	6-OMe	−3.7	−4.5
SO_3H	6-OMe	−4.4	−5.5

the lifetimes of nitrenium ions derived from AAB based compounds.

3.2. *OMe–AAB→N–OH–OMe–AAB→ N–OAc(OSO$_3$H)–OMe–AAB→ $^+$NH–OMe–AAB*

Since substitution of a methoxy group at the 3-position on AAB dramatically enhances its carcinogenic potency, whereas substitution of a methoxy group at the 2-position may even diminish its potency, we repeated our calculations for the analogous metabolites of *n*–OMe–AAB (*n* = 2, 3, 5 and 6). It was necessary to include 5-OMe–AAB (*ortho*) and 6-OMe–AAB (*meta*) in the calculations because these compounds are not identical to 3-OMe–AAB (*ortho*) and 2-OMe–AAB (*meta*) respectively; no distinction between substitution at the two *ortho* positions or at the two *meta* positions is generally made in the experimental literature.

It can be seen from Table 1 that methoxy substitution on AAB, N–OH–AAB, N–OAc–AAB (N–OSO$_3$H–AAB), and $^+$NH–AAB at an *ortho* position generally leads to lower-energy structures than methoxy substitution at a *meta* position. This can be understood by considering how methoxy substitution affects the energies of the frontier orbitals. For simplicity, we will concentrate our discussion on the *anti* forms. Methoxy substitution typically raises the Kohn–Sham frontier orbital energies of AAB and its metabolites, N–OH–AAB, N–OAc–AAB (N–OSO$_3$H–AAB) and $^+$NH–AAB, but the increase in energy is not the same for each orbital and depends on the position of the group. For example, methoxy substitution at the 2-position in these structures brings the oxygen and azo nitrogen lone pairs into close proximity and raises the energy of the azo lone-pair orbital (HOMO) substantially, ~10 kcal/mol, compared to the corresponding orbital in the

Table 5
Enthalpy change, ΔH (kcal/mol), for the reaction

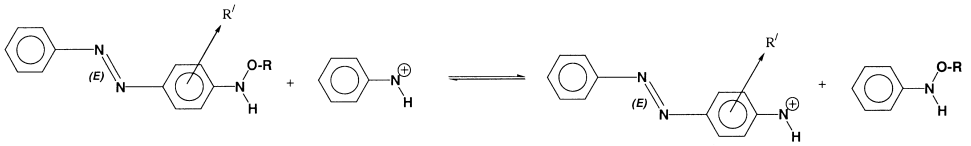

for A. R = H, Ac and SO_3H, R′ = H and B. R = H, Ac and SO_3H, R′ = 2(3)-OMe calculated at the BP/DN**//BP/DN** computational level

R	R′	ΔH (kcal/mol)	
		syn	*anti*
A.			
H	H	−25.7	−23.7
Ac	H	−27.1	−26.3
SO_3H	H	−26.3	−27.8
B.			
H	2-OMe	−34.2	−35.2
Ac	2-OMe	−36.0	−38.5
SO_3H	2-OMe	−35.8	−39.8
H	3-OMe	−36.1	−33.6
Ac	3-OMe	−37.0	−35.5
SO_3H	3-OMe	−36.6	−32.7
H	5-OMe	−34.8	−33.2
Ac	5-OMe	−36.0	−37.5
SO_3H	5-OMe	−34.3	−37.1
H	6-OMe	31.4	−30.8
Ac	6-OMe	−33.3	−33.4
SO_3H	6-OMe	−33.5	−34.0

unsubstituted structure; the energy of the amino lone-pair orbital (HOMO{-1}) is raised to a lesser extent, 3–5 kcal/mol. On the other hand, methoxy substitution at the 3(5)-position of these structures brings the oxygen atom closer to the amino nitrogen atom and raises the energy of the amino lone-pair orbital to a greater extent than it raises the energy of the azo lone-pair orbital (e.g. 4.9 kcal/mol compared to 0.9 kcal/mol for substitution at the 3-position). This greater increase in energy of the amino nitrogen lone pair orbital is sufficiently large to reverse the order of the Kohn–Sham HOMO{-1} and HOMO in 3(5)-OMe–AAB compared to that found in AAB and 2(6)-OMe–AAB. (This reversal of orbitals is not found in all the metabolites of 3-OMe–AAB, e.g. the order of the HOMO and HOMO{-1} in N–OSO_3H–3-OMe–AAB is similar to that found in AAB). Thus, in 3(5)-OMe–AAB the HOMO involves the amino nitrogen lone pair of electrons, which may facilitate its N-oxidation to N–OH-3(5)-OMe–AAB. Although this reversal of orbitals seems to have relatively little effect on the overall thermodynamics of the conversion from OMe–AAB to N–OH–OMe–AAB [8], it may influence the rate at which this process occurs. To explore this possibility further, we calculated a few topological and electronic indices of *n*-OMe–AAB ($n = 2$, 3, 5 and 6) using the program CODESSA in conjunction with the semiempincal AM1 method [37,38]; the results are given in Table 6A [49–51]. The atomic nucleophilic reactivity index, N_A, is defined as

$$N_A = \sum_{i \in A} (C_{i\mathrm{HOMO}})^2 / (1 - \varepsilon_{\mathrm{HOMO}}), \tag{3}$$

where the summation is performed over all atomic orbitals at a given atom, $C_{i\mathrm{HOMO}}$ denotes the *i*th atomic orbital coefficient on the highest occupied molecular orbital, and $\varepsilon_{\mathrm{HOMO}}$ is the energy of the HOMO. For the amino nitrogen atom, NA is found to be *greater* for 3(5)-OMe–AAB than for 2(6)-OMe–AAB, even though the calculated charge on this nitrogen atom is less negative for the 3(5)-isomer. It may also be noted that the value of N_A for unsubstituted AAB is between that of 3(5)-OMe–AAB and 2(6)-OMe–AAB. Interestingly, CODESSA finds that the maximum atomic nucleophilic reactivity index for a ring carbon atom is *greater* in 2(6)-OMe–AAB than in

Table 6
Topological and electronic indices calculated using CODESSA [37] in conjunction with AM1 [38] for A. AAB and *n*-OMe–AAB ($n = 2$, 3, 5 and 6) and B. $^+$NH–AAB and $^+$NH-2(3)-OMe–AAB

A.

Compound	Topological indices			Electronic indices		
	Wiener index [49]	Randic index (order 3) [50]	Balaban index [51]	Nucleophilic reactivity index		Partial charge
				Amino N	Ring C	Amino N
AAB	420.0	4.8433	2.1757	0.0192	0.0227	−0.3371
2-OMe–AAB	566.0	5.5969	2.2900	0.0139	0.0249	−0.3363
6-OMe–AAB	566.0	5.5969	2.2900	0.0138	0.0257	−0.3416
3-OMe–AAB	580.0	5.7034	2.2300	0.0210	0.0201	−0.3227
5-OMe–AAB	580.0	5.7034	2.2374	0.0199	0.0214	−0.3261

B.

Compound	Topological indices			Electronic indices	
	Wiener index [49]	Randic index (order 3) [50]	Balaban index [51]	Electrophilic reactivity index Amino N	Partial charge Amino N
$^+$NH–AAB	420.0	4.8433	2.0594	0.0419	−0.0705
$^+$NH–2-OMe–AAB	566.0	5.5969	2.1604	0.0339	−0.0942
$^+$NH-3-OMe–AAB	580.0	5.7034	2.2798	0.0443	−0.0541

3(5)-OMe–AAB, suggesting that detoxifying ring hydroxylation may be more significant in the noncarcinogenic 2(6)-positional isomer. Unfortunately, no direct experimental data on alternative oxidative products of AAB or OMe-AAB are currently available. Degawa et al. [52], however, have shown that the oxidative products of *O*-aminoazotoluene (OAT) include N–OH–OAT, 4′-OH–OAT and 2′-CH_2OH-3-Me–AAB.

The Kohn–Sham LUMOs of the nitrenium ions derived from 2-OMe–AAB and 3-OMe–AAB are shown in Fig. 4. Clearly the structure of these orbitals is somewhat different in the vicinity of C_4. The contribution to the LUMO at the amino nitrogen atom for $^+$NH–3-OMe–AAB is slightly greater than for $^+$NH–2-OMe–AAB, the orbital energy is slightly lower, and the calculated charge on the amino nitrogen atom for 3-OMe–AAB is less negative as compared to 2-OMe–AAB. In Table 6B we list the calculated atomic electrophilic reactivity index, E_A, for the amino nitrogen atom for these two nitrenium ions. This index is defined in CODESSA [37] as

$$E_A = \sum_{j \in A} \left(C_{j\mathrm{LUMO}}\right)^2 / (\varepsilon_{\mathrm{LUMO}} + 10.0), \tag{4}$$

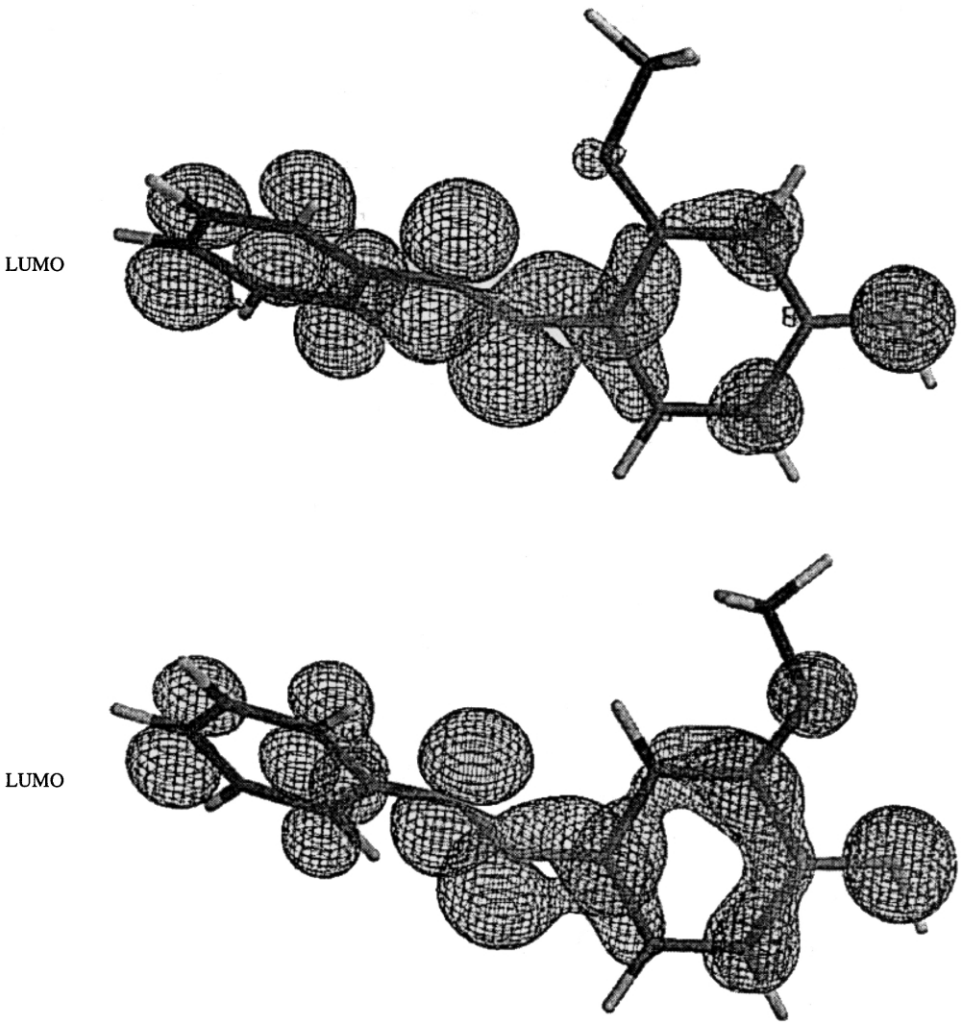

Fig. 4. The Kohn–Sham LUMO of $^+$NH-2-OMe–AAB and $^+$NH-3-OMe–AAB calculated at the BP/DN**//BP/DN** computational level.

where the summation is over all atomic orbitals at this atom, $C_{j\mathrm{LUMO}}$ denotes the jth atomic orbital coefficient on the lowest unoccupied orbital, and $\varepsilon_{\mathrm{LUMO}}$ is the energy of the LUMO. The value of E_A for the nitrenium ion derived from the potent carcinogen 3-OMe–AAB is *greater* than that for the nitrenium ion derived from the noncarcinogen 2-OMe–AAB (and for $^{+}$NH–AAB). Thus, $^{+}$NH–3-OMe–AAB may form DNA adducts more readily than $^{+}$NH–2-OMe–AAB. There is evidence [53] that N–OH–3-OMe–AAB gave 20-fold more DNA adducts than did N–OH–2-OMe–AAB although neither the structure of these adducts nor the mechanism of their formation was determined.

From Table 4B it can be seen that methoxy substitution has relatively little effect on the overall exothermicity for the reformation of the *N*-hydroxyl metabolite from the corresponding *N*-ester. On the other hand, from Table 5B it is clear that methoxy substitution stabilizes the resulting nitrenium ions by some 10 kcal/mol. For comparison we note that the energy change for reaction (2), using the *N*-hydroxide of the potent carcinogen 2-AF in place of N–OH–AAB, is −37.0 kcal/mol. Thus, methoxy substitution at either the *ortho* or *meta* positions in AAB yield nitrenium ions with stabilities comparable to those derived from 2-AAF.

In their study of the reactivity patterns of *N*-arylnitrenium ions, Novak et al. [27] observed a correlation between the logarithm of the rate constant ratio for competitive trapping of the nitrenium ions by the nucleophiles N_3^- and H_2O, log (K_{az}/K_s), and the enthalpy change for the reaction

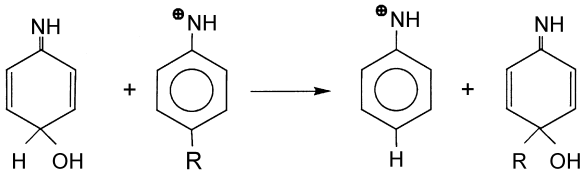

(4)

Taking R as –N=N–C_6H_5, we find the value of ΔH for this reaction to be rather large, +33 kcal/mol, which is similar in magnitude to the enthalpy change reported by Novak et al. [54] for the analogous reaction involving 2-AAF. Thus, $^{+}$NH–AAB can be expected to have a sufficiently long lifetime in an aqueous environment to react with other nucleophiles. For 2-OMe–AAB and 3-OMe–AAB the corresponding reaction enthalpies are larger, +37.2 and +39.6 kcal/mol respectively; the larger reaction enthalpy for 3-OMe–AAB would be expected to lead to the formation of more DNA adducts.

Finally, we note that many QSAR have found that the logarithm of the octanol–water partition coefficient, an indicator of hydrophobicity/hydrophilicity, plays an important role in regulating mutagenicity in the Ames Test [55]. Using the Ghose–Crippen approach [42] implemented in SPARTAN 5.0 [32] to calculate log P, we find that methoxy substitution on any of the AAB metabolites *decreases* its value by approximately 0.12 units, see Table 1, suggesting slightly greater hydrophilicity. These calculations, however, assume that log P is an additive constitutive molecular property [55] and they make no distinction between the positional isomers of OMe–AAB. Unfortunately no log P measurements have been reported in the literature for the compounds included in this study. In Table 7 we list the experimental values of log P for aniline and *n*-OMe–aniline (n = 2,3 and 4) [55]. Also included in this table are the corresponding values of log P calculated from SPARTAN 5.0 [32] and those calculated by Debnath et al. [55] using the CLOGP program [55]. These compounds are much more soluble in water than AAB or *n*-OMe–AAB which is reflected in significantly lower values of log P. It is evident from the experimental results that log P does depend on the position of the methoxy group, being largest for methoxy substitution at an *ortho* position. For aniline, SPARTAN overestimates log P by 0.33 units and

Table 7
Calculated and experimental values of log P for aniline and *n*-OMe–aniline (n = 2, 3 and 4)

Compound	Experimental	Calculated	
		CLOGP [55]	SPARTAN [32,42]
Aniline	0.90	0.92	1.23
2-OMe–aniline	1.18	1.02	1.10
3-OMe–aniline	0.93	1.02	1.10
4-OMe–aniline	0.95	1.02	1.10

finds that methoxy substitution *decreases* the calculated value of log *P*, contrary to the experimental results. The calculated value of log *P* for aniline, reported by Debnath et al. [55] is in better accord with experiment than that calculated from SPARTAN. Furthermore, these authors find that methoxy substitution *increases* log *P*. If the log *P* is also greater for methoxy substitution at an *ortho* position in AAB, this increased hydrophobicity would be another factor involved in the increased carcinogenic activity of 3-OMe–AAB [55]. Experimental values of log *P* for a collection of AAB dyes are needed. These values will help corroborate further computational results.

4. Conclusions

The carcinogenic activities of 2-OMe–AAB and 3-OMe–AAB are radically different [2]. Our calculations suggest that this difference may not be the result of a single factor along the metabolic pathway. Rather, we find several factors that appear to contribute to this difference:

- The Kohn–Sham HOMO of 3-OMe–AAB involves a contribution from the amino lone pair of electrons, whereas the HOMO of 2-OMe–AAB is concentrated at the azo linkage. Consistent with this, we find that the atomic nucelophilic reactivity index of the amino nitrogen atom is about 50% larger in 3-OMe–AAB than in 2-OMe–AAB. These results suggest that the critical initial step in the biotransformation of OMe–AAB may proceed faster for the carcinogen 3-OMe–AAB.
- The structures of the LUMOs of the nitrenium ions $^{+}$NH–3-OMe–AAB and $^{+}$NH–2-OMe–AAB are different, and the atomic electrophilic reactivity index of the amino nitrogen atom is about 30% greater in the ion derived from the carcinogen 3-OMe–AAB. This difference may influence the formation of DNA adducts.
- The maximum atomic nucleophilic index for a ring carbon atom is greater for 2-OMe–AAB than for 3-OMe–AAB suggesting that detoxifying ring hydroxylation may be more dominant in the noncarcinogen 2-OMe–AAB.

There is clearly much more we need to understand about the chemistry of the biotransformation of azo dyes and how this chemistry relates to carcinogenicity. We are currently investigating the structures, electronic features and binding energies of adducts involving the nitrenium ions derived from 2(3)-OMe–AAB and guanine. Differences in these adducts may suggest additional factors that influence the carcinogenic activities of 2-OMe–AAB and 3-OMe–AAB.

Acknowledgements

Dr. Krishna Bhat would like to thank the National Textile Center (Grant No. COO-POI) for financial support of this work.

References

[1] Miller JA. Carcinogensis by chemicals: an overview—G.H.A. Clowes Memorial Lecture. Cancer Res 1970;30:559.
[2] Kojima M, Degawa M, Hashimoto Y, Tada M. Biochem Biophy Res Commun 1991;179:817.
[3] Hashimoto Y, Degawa M, Watanabe HK, Tada M. Gann 1981;72:937.
[4] Kadlubar FF. In: Hemminki K, Dipple A, Shuker DEG, Kadlubar FF, Segerback D, Bartsch H, editors. DNA adducts of carcinogenic amines. Oxford, UK: University Press, 1994. p. 199–216.
[5] Schlichting I, Berendzen J, Chu K, Stock AM, Maves SA, Benson DE, Sweet RM, Ringe D, Petsko GA, Sligar SG. Science 2000;287:1615.
[6] Guengerich FP. J Biol Chem 1991;266:10019.
[7] Bhat KL, Freeman HS, Velga J, Sztandera L, Trachtman M, Bock CW. Dyes and Pigments 2000;46:109.
[8] Bhat KL, Trachtman M, Bock CW. Dyes and Pigments 2001;48:197.
[9] Ford GP, Herman PS. Chem Biol Interact 1992:1.
[10] Kimura T, Kodama M, Nagata C. Carcinogenesis 1982;3:1393.
[11] Kier LD, Brusick DJ, Auletta AE, Von Halle E, Brown MM, Simmon VF, Dunkel V, McCann J, Mortelmans K, Pnval M, Rao RK, Ray V. Muta Res 1986;169:69.
[12] Rosenkranz HS, Klopman G. Muta Res 1989;221:217.
[13] Cunningham AR, Klopman G, Rosenkranz HS. Muta Res 1998;405:9.

[14] Marroquin F, Coyote N. Chem Biol Interact 1970; 2:151.
[15] Irving CC, Veazey RA, Hill JT. Biochem Biophys Acta 1969;179:189.
[16] Garner RC, Martin CN, Clayson DB. In: Searle CE, editor. Chemical carcinogens, vol. 1, 2nd ed. ACS Monograph 182. Washington, DC: American Chemical Society, 1984. p. 175.
[17] Kriek E, Westra JG. In: Grover PL, editor. Chemical carcinogens and DNA, vol. 2. 1979. p. 1–28.
[18] Lin JK, Schmall B, Sharpe ID, Miuva I, Miller JA, Miller EC. Cancer Res 1975;35:832.
[19] Loew G, Sudhindra BS, Burt S, Pack GR, MacElroy X. Int J Quant Chem: Quant Bio Sym 1979;6:259.
[20] Miller EC. Cancer Res 1978;38:1479.
[21] Garner RC. Mutat Res 1998;402:67.
[22] Wang Z, Rizzo C. Org Letts 2001;3:565.
[23] Lin JK, Schmall B, Sharpe ID, Miura I, Miller JA, Miller EC. Cancer Res 1975;35:832.
[24] McClelland RA, Gadosy TA, Ren D. Can J Chem 1998; 76:1327.
[25] Novak M, Kahley MJ, Eiger E, Helmick JS, Peters HE. J Am Chem Soc 1993;115:9453.
[26] Novak M, Kahley MJ, Lin J, Kenneday SA, Swanegan LA. J Am Chem Soc 1994;116:11626.
[27] Novak M, Vandewater AJ, Brown AJ, Sanzenbacher SA, Hunt LA, Kolb BA, Brooks ME. J Org Chem 1999; 64:6023.
[28] Davidse PA, Kahley MJ, McClelland RA, Novak M. J Am Chem Soc 1994;116:45 13.
[29] McClelland RA, Davidse PA, Hadzialic G. J Am Chem Soc 1995;117:4173.
[30] Novak M, Kennedy SA. J Am Chem Soc 1995;117:574.
[31] Mohammad SN. Mol Pharmacol 1985;27:148.
[32] SPARTAN v5.0, Wavefunction Inc., 18401 Von Karmen Avenue, Suite 370, Irvine, CA 92612.
[33] Perdew JP. Phys Rev 1986;B33:8822.
[34] Perdew JP. Phys Rev 1987;B34:7046.
[35] Gill PMW, Johnson BG, Pople JA, Frisch M. J Chem Phys Lett 1992;197:499.
[36] Frisch MJ, Trucks GW, Schlegel HB, Scuseria GE, Robb MA, Cheeseman JR, et al. Gaussian 98. Revision A-7. Pittsburgh, PA: Gaussian Inc, 1998.
[37] Comprehensive descriptors for structural and statistical analysis (CODESSA), v2.0, Semichem, 7204 Mullen, Shawnee, KS 66216, USA.
[38] AMPAC 5.0, ©1994 Semichem, 7128 Summit, Shawnee, KS 66216.
[39] Katritzky AR, Lobanov VS, Karelson M. Chem Soc Rev 1995;24:279.
[40] Katritzky AR, Karelson M, Lobanov VS. Pure Appl Chem 1997;69:245.
[41] Menziani MC, DeBenedetti PG, Karelson M. Bioorg Med Chem 1998;6:535.
[42] Chase AK, Prittchett A, Crippen GM. J Comp Chem 1988;9:80.
[43] Hashimoto Y, Watanabe HK, Degawa M. Gann 1981; 72:921.
[44] Degawa M, Shoji Y, Masuko K, Hashimoto Y. Can Lett 1979;8:71.
[45] Parodi S, Taningher M, Russo P, Pala M, Tamaro M, Monti-Bragadin C. Carcinogenesis 1981;2:1317.
[46] Degawa M, Miyairi S, Hashimoto Y. Gann 1978;69:367.
[47] Scribner JD, Naimy NK. Can Res 1973;33:1159.
[48] McIlroy S, Cramer CJ, Falvey DE. Org Lett 2000; 2:2451.
[49] Wiener H. J Am Chem Soc 1947;69:17.
[50] Randic M. J Am Chem Soc 1975;97:6609.
[51] Balaban A. Pure Appl Chem 1983;55:199.
[52] Degawa M, Kanazawa C, Hashimoto Y. Carcinogenesis 1982;3:1113.
[53] Kojima M, Degawa M, Hashimoto Y, Tada M. Can Lett 1991;58:199.
[54] Novak M, Kazerani S. J Am Chem Soc 2000;122:3606.
[55] Debnath AS, Debnath G, Shusterman AJ, Hansch C. Environ Mol Mutagenesis 1992;19:37.